Particle Accelerators, 1973, Vol. 4, pp. 169–186

PHOTON DOSE RATES FROM THE INTERACTIONS OF 200-GeV PROTONS IN IRON AND IRON–LEAD BEAM STOPS†

T. A. GABRIEL AND R. T. SANTORO

Oak Ridge National Laboratory, Oak Ridge, Tennessee, 37830, USA

The calculated photon dose rates from the long-lived ($\tau_{1/2} > 1$ min) photon- and positron-emitting radioactive nuclides produced when 200-GeV protons are incident on a semi-infinite cylindrical iron beam stop having a radius of 40.64 cm (16 in.) are compared with the calculated photon dose rates from long-lived photon- and positron-emitting radioactive nuclides produced by 200-GeV protons in semi-infinite beam stops having a 30.48-cm (12 in.) radius iron core but surrounded by either 5.08 cm (2 in.) or 10.16 cm (4 in.) of lead. Data are also presented comparing the calculated photon dose rates from the long-lived photon- and positron-emitting radioactive nuclides produced when 200-GeV protons are incident on semi-infinite cylindrical iron beam stops having radii of 10.16 cm (4 in.), 20.32 cm (8 in.), 30.48 cm (12 in.), and 40.64 cm (16 in.).

1. INTRODUCTION

The photon dose rates from photon- and positron-emitting radioactive residual nuclides produced by sustained bombardment of accelerator beam stops by high-energy protons may present a significant radiation hazard to personnel and equipment in the vicinity of the beam stops. In order to minimize this hazard, the shielding engineer must know not only the magnitude of these dose rates but also how these dose rates change with energy, material, geometry, and time. In the results reported here, the calculated photon dose rates from the long-lived ($\tau_{\frac{1}{2}} > 1$ min) photon- and positron-emitting radioactive nuclides produced when 200-GeV protons are incident on a semi-infinite cylindrical iron beam stop having a radius of 40.64 cm (16 in.) are compared with the calculated photon dose rates from long-lived photon- and positron-emitting radioactive nuclides produced by 200-GeV protons in semi-infinite beam stops having a 30.48-cm (12-in.) radius iron core but surrounded by either 5.08 cm (2 in.) or 10.16 cm (4 in.) of lead. Data are also presented comparing the calculated photon dose rates from the long-lived photon- and positron-emitting radioactive nuclides produced when 200-GeV protons are incident on semi-infinite cylindrical iron beam stops having radii of 10.16 cm (4 in.), 20.32 cm (8 in.), 30.48 cm (12 in.), and 40.64 cm (16 in.), respectively.

† This research was funded by the U.S. Atomic Energy Commission under contract with Union Carbide Corporation.

The methods of calculation are discussed in Sec. 2, the results are presented in Sec. 3, and a summary of the conclusions is presented in Sec. 4.

2. METHODS OF CALCULATION

A schematic diagram showing the coordinate system and composition of the beam stops considered in this study is given in Fig. 1. The isotopic composition and density of the iron and lead were taken to be those that occur naturally.

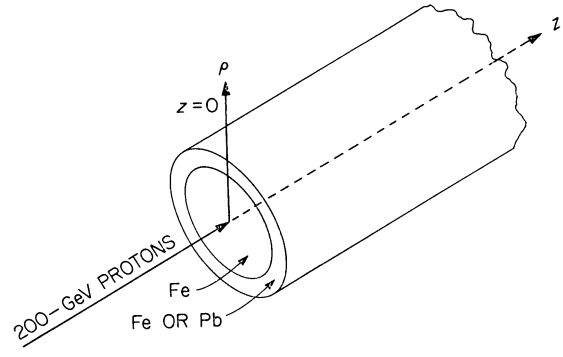

FIG. 1. Geometry and composition of the beam stop.

The three-dimensional high-energy nucleon-meson transport code HETC[1] was used to obtain a detailed description of the nucleon and meson cascade produced by the 200-GeV proton reactions in the beam stops. This Monte Carlo code takes into account the slowing down of charged particles

via the continuous slowing-down approximation, the decay of charged pions and muons, nonelastic nucleon- and charged-pion-nucleus (excluding hydrogen) collisions through the intranuclear-cascade-evaporation model[2] ($E \lesssim 3$ GeV) and the extrapolation-evaporation model[3] ($E \gtrsim 3$ GeV), nonelastic nucleon- and charged-pion-hydrogen collisions via the isobar model[4] ($E \lesssim 3$ GeV) and phenomenological fits to experimental data[5] ($E \gtrsim 3$ GeV), elastic neutron-nucleus collisions ($E \lesssim 100$ MeV), and elastic nucleon- and charged-pion-hydrogen collisions. In the HETC calculations, nucleons were transported to 15 MeV and charged pions were transported to ~ 2 MeV with negative pions being captured when they slowed down to their cutoff energy.

For the transport of neutrons below 15 MeV and of γ-rays from decaying nuclei, the three-dimensional multigroup neutron and γ-ray Monte Carlo transport code MORSE[6] was used. The neutron cross-section data required in MORSE were obtained from Refs. 7 and 8. The γ-ray cross-section data for use in MORSE were obtained from the computer code MUG,[9] which utilizes the Klein-Nishina formula and the OGRE[10] library tape.

The spatial dependence of the photon- and positron-emitting radioactive nuclides required to define the source kernel for the γ-ray transport was obtained by a direct analysis of the information generated by HETC. The production of these radioactive nuclides by neutrons with energy $\leqq 15$ MeV was obtained when needed by integrating over neutron energy the product of the neutron flux per unit energy obtained from MORSE and the macroscopic residual nuclide-production cross sections.[11]

The production of a given nuclide can also result from the decay of another nucleus that was produced in a nuclear interaction (by one or several decay steps). For the problem considered here, this mode of radioactive nuclide production in iron is relatively insignificant and has been ignored. For some of the radioactive nuclides produced in lead, however, this production mode is important and has been included in these calculations.

To obtain the time dependence of the buildup and decay of activity, it was assumed that the proton beam was turned on at time zero and maintained at a constant intensity until shutdown. For a nuclide produced directly from a nuclear interaction and not produced by the decay of another nuclide, the time dependence of the dose rate is given by

$$D_j(\mathbf{r}, t_i, t_S) = D_j(\mathbf{r}, \infty, 0)[1-\exp(-\ln 2t_i/\tau_{\frac{1}{2}j})] \cdot \exp(-\ln 2t_S/\tau_{\frac{1}{2}j}), \quad (1)$$

where

$D_j(\mathbf{r}, t_i, t_S)$ = the dose at $\mathbf{r}$ associated with the jth nuclide of half life $\tau_{\frac{1}{2}j}$ for an irradiation time t_i and a time after shutdown of t_S, and

$D_j(\mathbf{r}, \infty, 0)$ = the dose rate $\mathbf{r}$ from the jth nuclide produced directly from nuclear interactions following an infinite irradiation time and zero shutdown time.

For a nuclide produced not only from a nuclear interaction but also by the decay of another nuclide, the time dependence of the dose rate is given by

$$D_j(\mathbf{r}, t_i, t_S) = D_j(\mathbf{r}, \infty, 0)\left[\frac{1}{K}(T_1+T_2+T_3)+T_4\right], \quad (2)$$

where

$$T_1 = \frac{[1-\exp(-\ln 2t_i/\tau_{\frac{1}{2}k})][\exp(-\ln 2t_S/\tau_{\frac{1}{2}k}) - \exp(-\ln 2t_S/\tau_{\frac{1}{2}j})]\tau_{\frac{1}{2}k}}{\tau_{\frac{1}{2}k}-\tau_{\frac{1}{2}j}},$$

$$T_2 = [1-\exp(-\ln 2t_i/\tau_{\frac{1}{2}j})]\exp(-\ln 2t_S/\tau_{\frac{1}{2}j}),$$

$$T_3 = \frac{\tau_{\frac{1}{2}k}}{\tau_{\frac{1}{2}k}-\tau_{\frac{1}{2}j}}[\exp(-\ln 2t_i/\tau_{\frac{1}{2}j})-\exp(-\ln 2t_i/\tau_{\frac{1}{2}k})] \cdot \exp(-\ln 2t_S/\tau_{\frac{1}{2}j}),$$

and

$$T_4 = [1-\exp(-\ln 2t_i/\tau_{\frac{1}{2}j})]\exp(-\ln 2t_S/\tau_{\frac{1}{2}j}).$$

In these equations $\tau_{\frac{1}{2}k}$ equals the half-life of a nuclide of type k that will decay into a nuclide of type j, and K is the ratio of the number of nuclides of type j produced per second to the number of nuclides of type k produced per second that will decay into j. All other terms have been defined previously.

The γ-ray source spectra from each of the nuclides considered were taken from the Nuclear Data Sheets[12], and the γ-ray flux-to-dose-rate conversion factors were obtained elsewhere.[13]

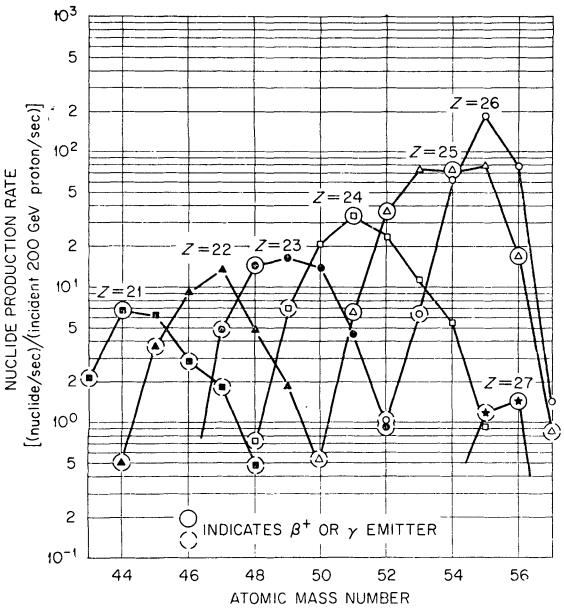

FIG. 2. Selected nuclide-production rates for incident 200-GeV protons in a semi-infinite iron cylinder of 40.64-cm radius.

TABLE I

Selected Nuclide-Production Rates in a 10.16-cm Lead Collar Surrounding a 200-GeV Proton Iron Beam Stop Having a Radius of 30.48 cm

	Nuclides/sec/incident 200-GeV proton/sec	
Atomic Mass	^{81}Tl	^{82}Pb
195	2.68×10^{-1}	2.61×10^{-1}
196	2.32×10^{-1}	1.12×10^{-1}
197	2.13×10^{-1}	5.42×10^{-1}
198	2.76×10^{-1}†	6.98×10^{-1}†
199	3.29×10^{-1}†	8.56×10^{-1}†
200	2.58×10^{-1}†	1.27×10^{0} †
201	4.13×10^{-1}	2.17×10^{0} †
202	5.26×10^{-1}†	2.74×10^{0} †
203	3.78×10^{-1}	3.25×10^{0} †
204	8.23×10^{-1}	4.37×10^{0} †
205	6.34×10^{-1}	6.43×10^{0}
206	6.96×10^{-1}	8.23×10^{0}
207	9.73×10^{-1}	4.10×10^{0}
208	6.74×10^{-2}	3.54×10^{0}

† The radioactive nuclides considered in obtaining the photon dose rates.

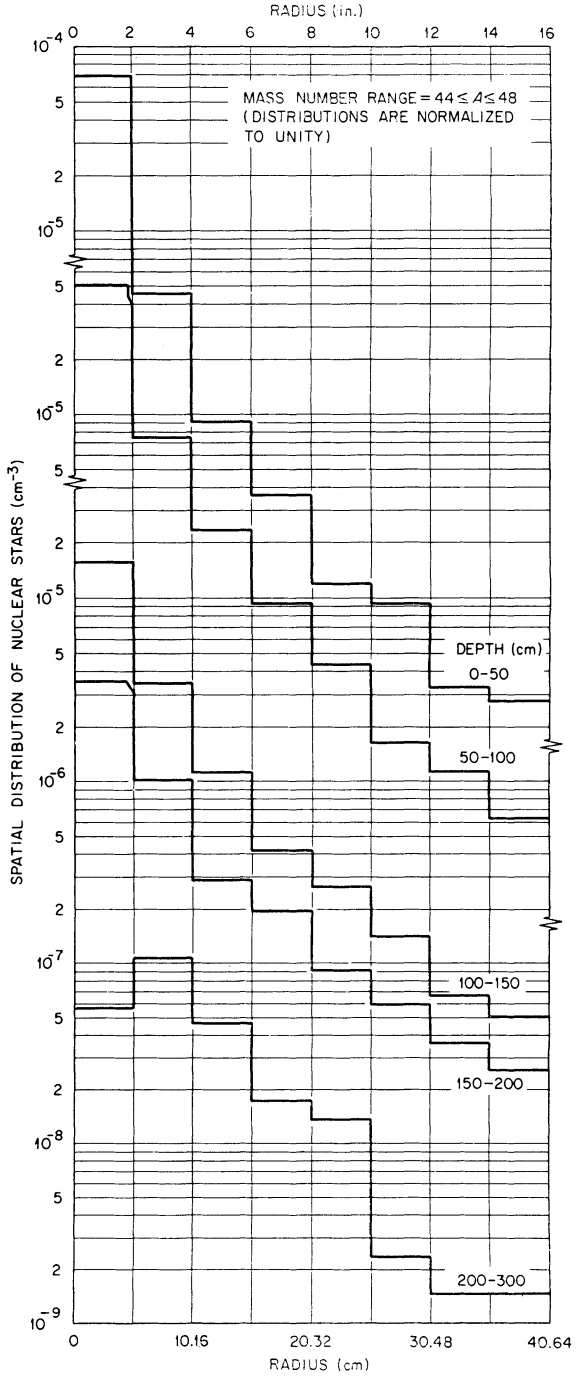

FIG. 3. Normalized spatial distributions of nuclear stars in the atomic mass range $44 \leqq A \leqq 48$ produced in iron by 200-GeV protons.

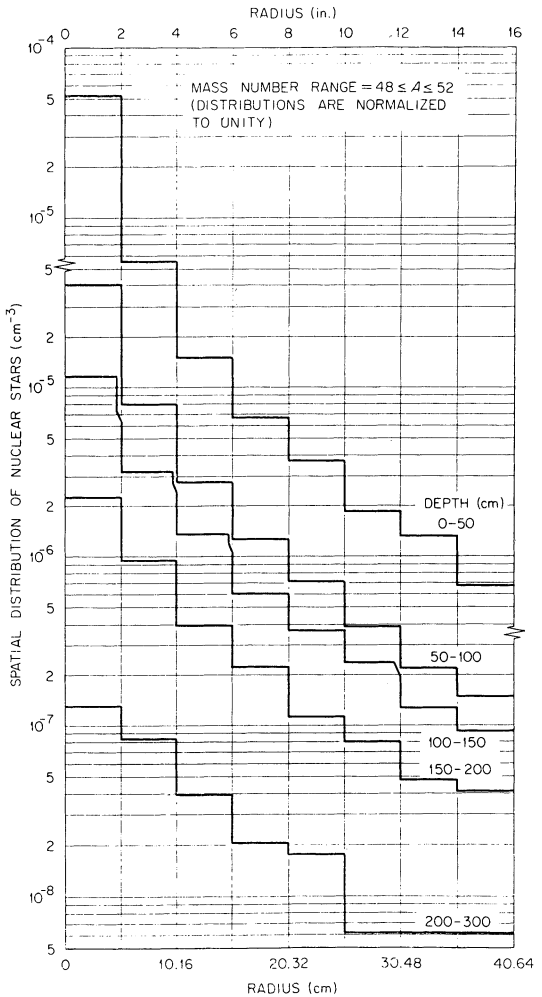

FIG. 4. Normalized spatial distributions of nuclear stars in the atomic mass range $48 \leqq A \leqq 52$ produced in iron by 200-GeV protons.

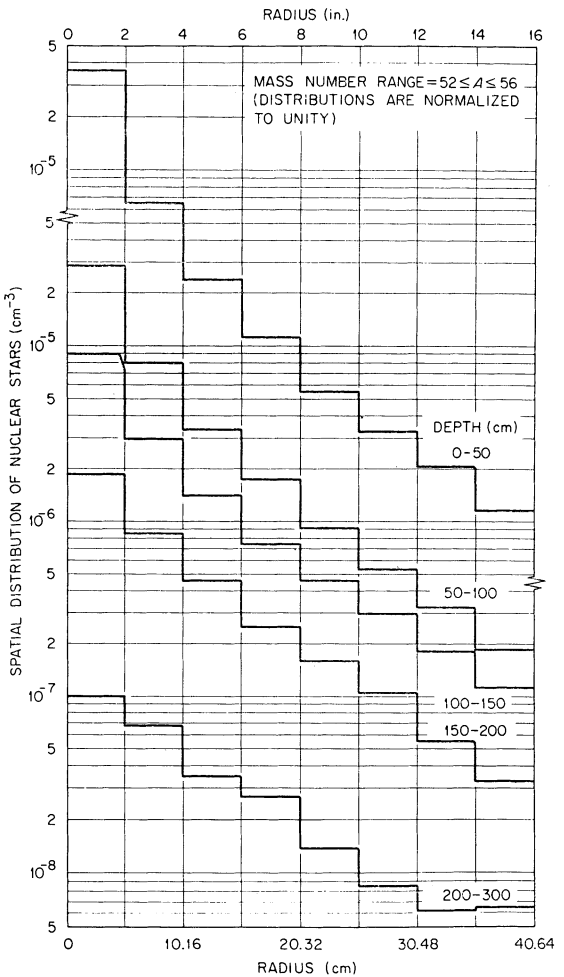

FIG. 5. Normalized spatial distributions of nuclear stars in the atomic mass range $52 \leqq A \leqq 56$ produced in iron by 200-GeV protons.

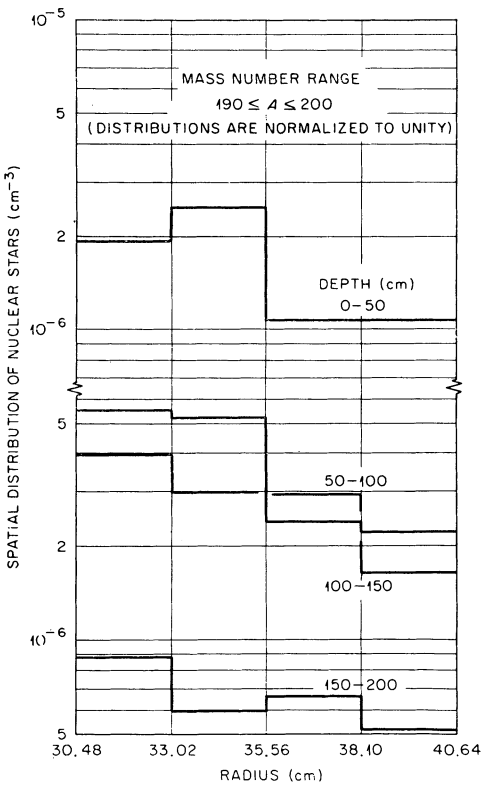

FIG. 6. Normalized spatial distributions of nuclear stars in the atomic mass range $190 \leqq A \leqq 200$ produced in a 10.16-cm lead collar surrounding a 200-GeV proton beam stop composed of iron and having a radius of 30.48 cm.

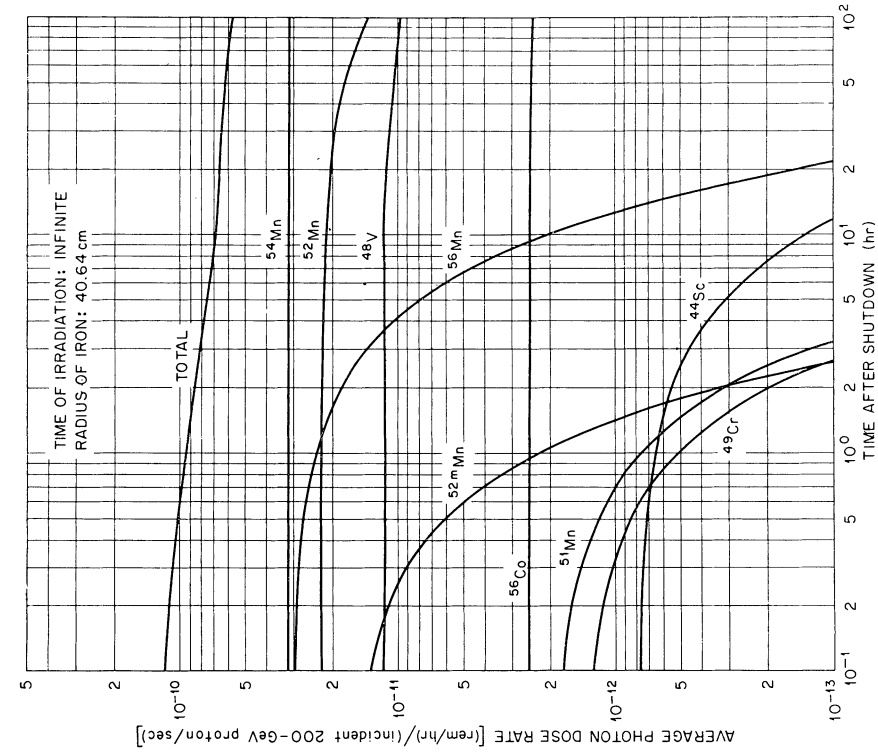

FIG. 8. Contribution of various radionuclides to the average total photon dose rate. Beam stop is composed of iron and has a radius of 40.64 cm.

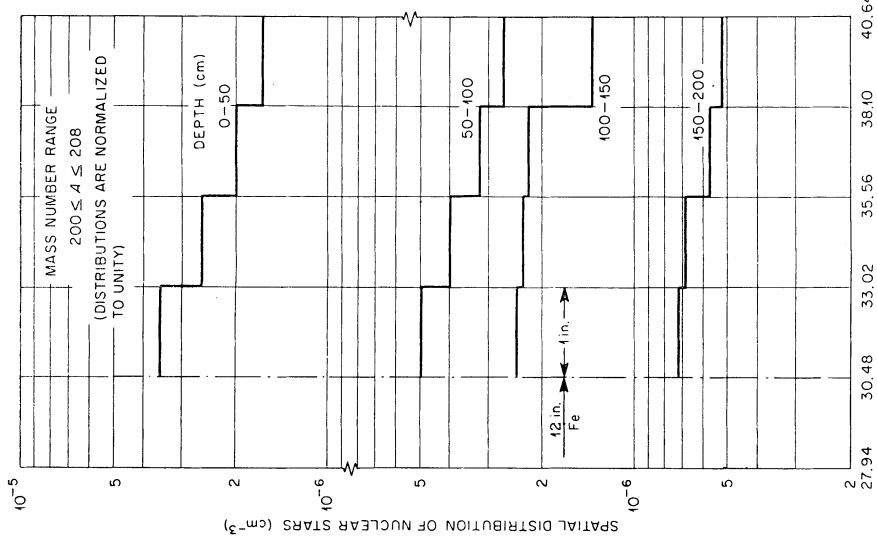

FIG. 7. Normalized spatial distributions of nuclear stars in the atomic mass range $200 \leqq A \leqq 208$ produced in a 10.16-cm lead collar surrounding a 200-GeV proton beam stop composed of iron and having a radius of 30.48 cm.

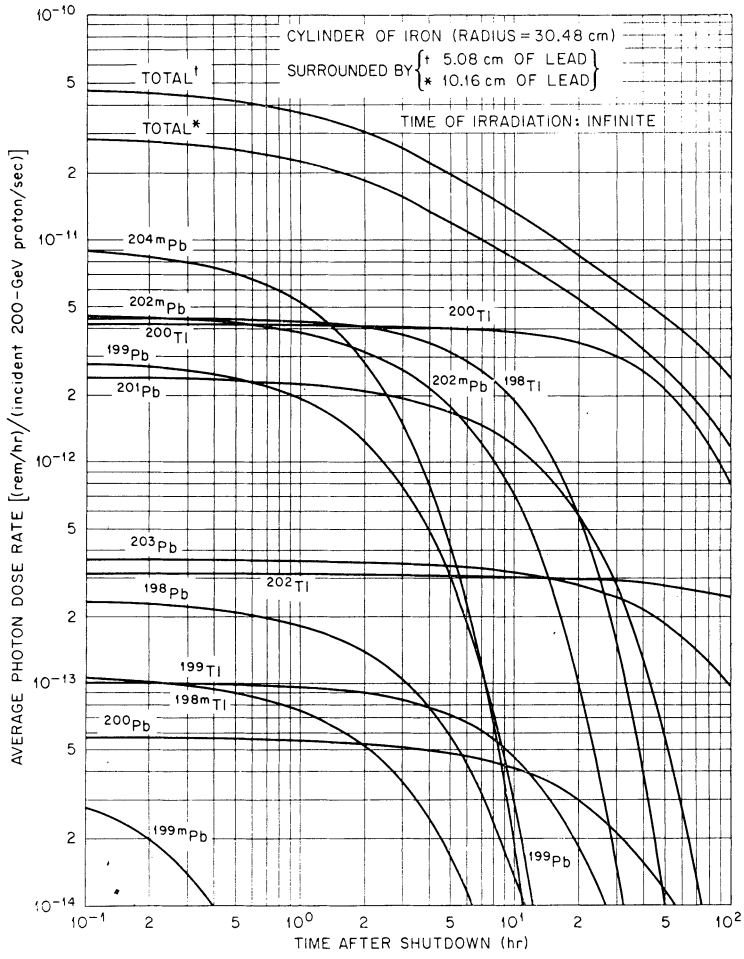

FIG. 9. Contribution of various radionuclides to the average total photon dose rate. Beam stop is composed of an iron cylinder of 30.48-cm radius surrounded by 10.16 cm of lead. Also shown is the average total photon dose rate for the 5.08-cm lead collar case.

3. RESULTS

The production rate of selected nuclides per incident 200-GeV proton per second in a semi-infinite iron beam stop of 40.48-cm radius by nucleons with energies > 15 MeV and pions with energies > 2.2 MeV (including negative-pion capture) as a function of atomic mass number A and parameterized by atomic number Z is given in Fig. 2. The long-lived ($\tau_{\frac{1}{2}} > 1$ min) photon- and positron-emitting radioactive nuclides considered in this study are inscribed by the solid circles. The lesser important nuclides are inscribed by the dashed circles, and estimates of the dose rates from these nuclides can be found in Ref. 14. The isotopes ^{56}Mn and ^{54}Mn, which are of interest in calculating the photon dose rates, are produced in nonnegligible quantities by neutrons below 15 MeV. The production of these isotopes by low-energy neutrons was calculated to be 21.9 and 20.8 nuclides per second per incident 200-GeV proton per second, respectively.

To simplify and summarize the spatial dependence of the nuclide production rates presented in Fig. 2, normalized spatial distributions for the atomic mass ranges of $44 \leqq A \leqq 48$, $48 \leqq A \leqq 52$, and $52 \leqq A \leqq 56$ are plotted in Figs. 3–5. These distributions can be used in conjunction with the data of Fig. 2 to obtain a reasonable estimate of the spatial dependence of the production rate for a particular nuclide.

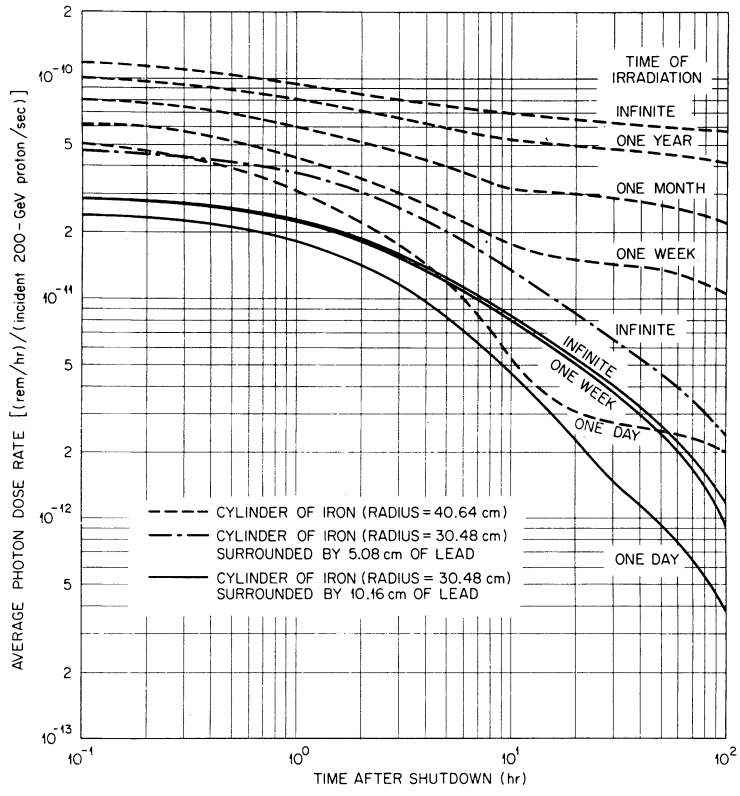

FIG. 10. Comparison of the average total photon dose rates for cases 1, 2, and 3 for several irradiation times.

The production rates of selected nuclides in the 10.16-cm lead collar surrounding the 30.48-cm radius iron beam stop are listed in Table I. Only lead and thallium isotopes are listed since they represent the significant reaction products. The production rates of other nuclides were obtained but were not needed for the present problem. The spatial dependence of these nuclides is summarized in Figs. 6 and 7 for the atomic mass ranges of $190 \leqq A \leqq 200$ and $200 \leqq A \leqq 208$, respectively.

The total photon dose rate averaged over the first 200 cm along the edge of the beam stop and the individual contributors to the total dose rate as a function of shutdown following an infinite irradiation time are shown in Fig. 8 for the 40.64-cm radius iron beam stop (case 1). The data have been normalized to one incident 200-GeV proton per second. In the production of ^{44}Sc and ^{52}Mn, two isomeric states are formed. Since the calculated production rates include both isomers, and the relative contributions cannot be distinguished, it was assumed that each isomer was produced in equal amounts. This assumption is applied to all other isomeric states that are formed.

The average photon dose rates as a function of shutdown time following an infinite irradiation time for the 30.48-cm radius iron beam stop surrounded by 5.08 cm (case 2) and 10.16 cm (case 3) of lead are shown in Fig. 9. Only the average total photon dose rate is shown for case 2. The individual contributors shown are for case 3. The same HETC transport results for case 3 were used for case 2 by removing from consideration in the γ-ray transport the outer 5.08 cm of lead.

Comparing the average total dose rates in Figs. 8 and 9 leads to the conclusion that the lead collar substantially reduces the average total dose rate. For case 3, the average total dose rate from the active nuclides produced in the iron is insignificant. Some contribution ($\sim$ 10–30 per cent) from these

nuclides is observed in case 2, and this contribution has been included in the total-dose-rate curve shown in Fig. 9.

Another comparison of the average total photon dose rates for the three cases discussed above is shown in Fig. 10. For this comparison, several irradiation times have been considered. As observed in Fig. 10, an additional advantage of surrounding the iron with lead is that the cooling rate is more rapid for the residual nuclei produced in the lead than for those produced in the iron.

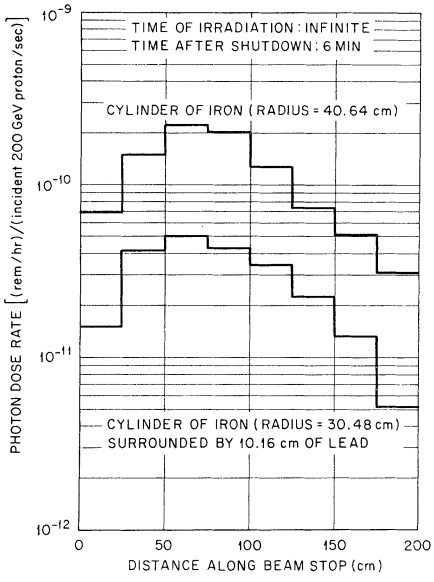

FIG. 11. Spatial dependence of the photon dose rates for cases 1 and 3.

The variations of the dose rates for cases 1 and 3 as a function of position along the edge of the beam stop are shown in Fig. 11. These data, which are of prime interest in shielding, show the peak photon dose rates at six minutes after shutdown following an infinite irradiation time. The peak photon dose rates are approximately a factor of two larger than the average dose rates shown in Figs. 8 and 9.

Tables II–VI summarize the data for the various nuclides that contribute to the total photon dose rate, the photon leakage flux, and the photon leakage flux per unit energy for cases 1, 2, and 3. These data were computed at zero shutdown time† following an infinite irradiation time. Tables II and IV give the spatial dependence of the dose rates from the individual nuclides for cases 1 and 3, respectively. These tables also include the individual contributors to the photon leakage flux. The line labeled 'albedo' in each table gives the photon dose or leakage flux from the front face of the beam stop. In Tables III and V, the photon leakage spectra have been normalized to unity and, in application, must be renormalized by the corresponding photon leakage flux values given in Tables II and IV. The normalized data in Tables III and V were obtained by evaluating the spectra over the first 200 cm along the edge of the beam stop. Using the photon leakage flux values, renormalization will yield reasonable estimates of the spatial dependence of the photon leakage flux per unit energy.

The results in Table VI are the average dose rates and average photon leakage flux for case 2. The spatial dependence of the dose rates and photon leakage flux for this case are similar to the results obtained for corresponding nuclei presented in Tables II and IV.

The data obtained for the lead nuclides in Tables IV and VI are the dose rates from the nuclides produced directly by nuclear interaction. To include the contribution from nuclide decay, Eq. 2 and the values of K specified in the tables must be used.

The average photon dose rate for an infinite irradiation time and zero shutdown time as a function of beam-stop radius is shown in Fig. 12.

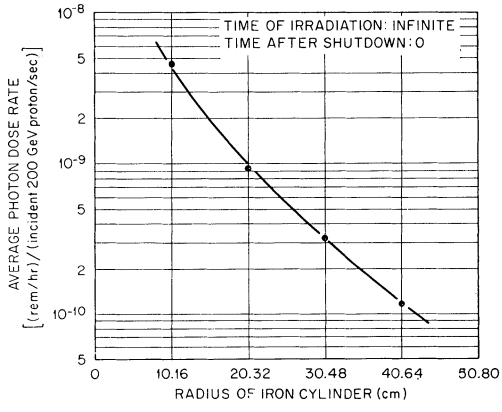

FIG. 12. Dependence of the average photon dose rate on the radius of an iron beam stop.

† Since short-lived nuclides have not been considered, these results should be used in conjunction with Eqs. (1) and (2) for $t_S \geqq 6$ minutes.

TABLE II

Spatial Dependence of the Photon Dose Rates and Photon Leakage Fluxes for Selected Residual Nuclides Produced by 200-GeV Protons in an Iron Cylinder of 40.64-cm Radius

Distance Along Cylinder (cm)	Photon Dose Rate[a] [(rem/h)/(incident 200-GeV proton/sec)]								
	^{56}Co	^{56}Mn	^{54}Mn	^{52}Mn	^{52m}Mn	^{51}Mn	^{49}Cr	^{48}V	^{44}Sc
0- 25	1.65×10^{-12}	1.84×10^{-11}	2.33×10^{-11}	1.44×10^{-11}	9.79×10^{-12}	1.28×10^{-12}	3.36×10^{-13}	3.00×10^{-12}	9.00×10^{-14}
25- 50	3.14×10^{-12}	4.18×10^{-11}	4.29×10^{-11}	2.68×10^{-11}	1.93×10^{-11}	2.82×10^{-12}	1.11×10^{-12}	1.19×10^{-11}	1.40×10^{-12}
50- 75	4.18×10^{-12}	5.52×10^{-11}	6.11×10^{-11}	3.95×10^{-11}	3.07×10^{-11}	2.91×10^{-12}	2.51×10^{-12}	3.08×10^{-11}	1.37×10^{-12}
75-100	4.09×10^{-12}	4.88×10^{-11}	4.59×10^{-11}	4.52×10^{-11}	3.29×10^{-11}	3.20×10^{-12}	3.62×10^{-12}	2.39×10^{-11}	1.34×10^{-12}
100-125	3.04×10^{-12}	3.55×10^{-11}	3.60×10^{-11}	2.51×10^{-11}	1.52×10^{-11}	2.11×10^{-12}	1.06×10^{-12}	8.54×10^{-12}	5.20×10^{-13}
125-150	1.80×10^{-12}	2.41×10^{-11}	1.98×10^{-11}	1.33×10^{-11}	8.47×10^{-12}	8.11×10^{-13}	8.76×10^{-13}	6.52×10^{-12}	5.40×10^{-13}
150-175	1.16×10^{-12}	1.35×10^{-11}	1.49×10^{-11}	8.03×10^{-12}	8.53×10^{-12}	1.06×10^{-12}	9.27×10^{-13}	4.36×10^{-12}	8.63×10^{-13}
175-200	9.47×10^{-13}	7.53×10^{-12}	8.92×10^{-12}	6.50×10^{-12}	3.50×10^{-12}	8.66×10^{-13}	6.30×10^{-13}	2.67×10^{-12}	9.59×10^{-14}
Average	2.50×10^{-12}	3.06×10^{-11}	3.16×10^{-11}	2.24×10^{-11}	1.61×10^{-11}	1.88×10^{-12}	1.38×10^{-12}	1.15×10^{-11}	7.77×10^{-13}
Albedo	8.44×10^{-12}	1.08×10^{-10}	1.28×10^{-10}	6.39×10^{-11}	5.20×10^{-11}	7.80×10^{-12}	5.66×10^{-12}	5.94×10^{-11}	9.19×10^{-12}

Distance Along Cylinder (cm)	Photon Leakage Flux[a] [(photons/sec·cm^2)/(incident 200-GeV proton/sec)]								
	^{56}Co	^{56}Mn	^{54}Mn	^{52}Mn	^{52m}Mn	^{51}Mn	^{49}Cr	^{48}V	^{44}Sc
0- 25	9.88×10^{-7}	1.21×10^{-5}	1.76×10^{-5}	9.03×10^{-6}	7.11×10^{-6}	1.38×10^{-6}	3.86×10^{-7}	2.13×10^{-6}	8.00×10^{-8}
25- 50	1.91×10^{-6}	2.63×10^{-5}	3.19×10^{-5}	1.90×10^{-5}	1.47×10^{-5}	3.05×10^{-6}	1.30×10^{-6}	8.44×10^{-6}	1.18×10^{-6}
50- 75	2.60×10^{-6}	3.24×10^{-5}	4.82×10^{-5}	2.81×10^{-5}	2.37×10^{-5}	3.25×10^{-6}	2.77×10^{-6}	1.98×10^{-5}	1.11×10^{-6}
75-100	2.50×10^{-6}	2.93×10^{-5}	3.63×10^{-5}	3.13×10^{-5}	2.55×10^{-5}	3.56×10^{-6}	3.84×10^{-6}	1.79×10^{-5}	1.12×10^{-6}
100-125	1.73×10^{-6}	2.03×10^{-5}	2.93×10^{-5}	1.84×10^{-5}	1.17×10^{-5}	2.38×10^{-6}	1.23×10^{-6}	6.43×10^{-6}	4.69×10^{-7}
125-150	1.04×10^{-6}	1.45×10^{-5}	1.61×10^{-5}	1.05×10^{-5}	6.43×10^{-6}	9.44×10^{-7}	1.02×10^{-6}	5.11×10^{-6}	4.72×10^{-7}
150-175	7.23×10^{-7}	8.35×10^{-6}	1.15×10^{-5}	5.26×10^{-6}	5.63×10^{-6}	1.12×10^{-6}	1.06×10^{-6}	3.19×10^{-6}	6.93×10^{-7}
175-200	4.84×10^{-7}	3.99×10^{-6}	6.74×10^{-6}	4.33×10^{-6}	3.29×10^{-6}	9.25×10^{-7}	6.91×10^{-7}	1.79×10^{-6}	1.01×10^{-7}
Average	1.50×10^{-6}	1.84×10^{-5}	2.47×10^{-5}	1.57×10^{-5}	1.23×10^{-5}	2.08×10^{-6}	1.54×10^{-6}	8.09×10^{-6}	6.53×10^{-7}
Albedo	5.61×10^{-6}	6.66×10^{-5}	9.39×10^{-5}	4.68×10^{-5}	3.90×10^{-5}	8.56×10^{-6}	6.06×10^{-6}	4.40×10^{-5}	7.90×10^{-6}

a. Time of irradiation = infinite;
Time after shutdown = 0 (see footnote on page 18).

TABLE III

Energy Dependence of the Averaged Normalized Photon Leakage Flux Per Unit Energy for Selected Residual Nuclides Produced by 200-GeV Protons in an Iron Cylinder of 40.64-cm Radius

Energy Interval (MeV)	Normalized Photon Leakage Flux Per Unit Energy[a] (MeV^{-1})								
	^{56}Co	^{56}Mn	^{54}Mn	^{52}Mn	^{52m}Mn	^{51}Mn	^{49}Cr	^{48}V	^{44}Sc
4.00 -3.28	1.41×10^{-2}	1.79×10^{-3}							
3.28 -2.68	3.27×10^{-2}	2.68×10^{-3}							
2.68 -2.20	8.88×10^{-2}	3.32×10^{-2}						1.64×10^{-2}	
2.20 -1.80	6.96×10^{-2}	3.38×10^{-1}						2.71×10^{-3}	
1.80 -1.47	9.47×10^{-2}	1.90×10^{-1}			1.60×10^{-1}			3.31×10^{-4}	
1.47 -1.21	4.33×10^{-1}	7.09×10^{-2}		6.55×10^{-1}	5.53×10^{-1}			7.22×10^{-1}	
1.21 -0.988	3.74×10^{-1}	1.04×10^{-1}		8.43×10^{-2}	1.34×10^{-1}			3.14×10^{-1}	7.32×10^{-1}
0.988 -0.809	8.41×10^{-1}	1.26×10^{0}	1.87×10^{0}	7.76×10^{-1}	1.36×10^{-1}			6.16×10^{-1}	1.22×10^{-1}
0.809 -0.663	4.58×10^{-1}	5.08×10^{-1}	1.12×10^{0}	1.02×10^{0}	1.90×10^{-1}			3.91×10^{-1}	4.02×10^{-1}
0.663 -0.543	4.06×10^{-1}	5.74×10^{-1}	6.50×10^{-1}	5.21×10^{-1}	2.21×10^{-1}			3.41×10^{-1}	3.78×10^{-1}
0.543 -0.445	1.09×10^{0}	5.50×10^{-1}	8.03×10^{-1}	1.18×10^{0}	3.08×10^{0}	4.70×10^{0}	4.86×10^{0}	1.76×10^{0}	3.03×10^{0}
0.445 -0.364	8.06×10^{-1}	6.92×10^{-1}	6.57×10^{-1}	9.59×10^{-1}	1.08×10^{0}	1.44×10^{0}	1.10×10^{0}	9.71×10^{-1}	1.14×10^{0}
0.364 -0.298	6.93×10^{-1}	9.84×10^{-1}	9.13×10^{-1}	8.87×10^{-1}	1.13×10^{0}	1.32×10^{0}	1.57×10^{0}	7.55×10^{-1}	1.38×10^{0}
0.298 -0.244	9.14×10^{-1}	9.93×10^{-1}	1.22×10^{0}	1.15×10^{0}	1.08×10^{0}	1.79×10^{0}	1.65×10^{0}	1.24×10^{0}	1.18×10^{0}
0.244 -0.200	1.08×10^{0}	1.33×10^{0}	1.61×10^{0}	1.15×10^{0}	1.41×10^{0}	1.82×10^{0}	1.43×10^{0}	1.56×10^{0}	1.47×10^{0}
0.200 -0.164	1.04×10^{0}	9.50×10^{-1}	1.29×10^{0}	1.10×10^{0}	1.61×10^{0}	2.19×10^{0}	2.15×10^{0}	8.08×10^{-1}	1.42×10^{0}
0.164 -0.134	8.84×10^{-1}	9.15×10^{-1}	9.29×10^{-1}	1.16×10^{0}	9.95×10^{-1}	1.44×10^{0}	1.54×10^{0}	1.23×10^{0}	8.95×10^{-1}
0.134 -0.110	7.96×10^{-1}	5.43×10^{-1}	5.73×10^{-1}	4.38×10^{-1}	4.63×10^{-1}	8.84×10^{-1}	1.15×10^{0}	4.92×10^{-1}	5.86×10^{-1}
0.110 -0.0900	3.14×10^{-1}	2.21×10^{-1}	3.64×10^{-1}	2.48×10^{-1}	3.84×10^{-1}	3.73×10^{-1}	8.50×10^{-1}	3.33×10^{-1}	3.48×10^{-1}
0.0900-0.0737	6.04×10^{-2}	6.71×10^{-2}	6.35×10^{-2}	4.29×10^{-2}	1.47×10^{-1}	2.27×10^{-1}	2.95×10^{-1}	7.34×10^{-2}	1.91×10^{-1}
0.0737-0.0603	1.38×10^{-2}	8.83×10^{-3}	2.80×10^{-3}	1.19×10^{-2}	4.87×10^{-3}	9.91×10^{-3}	3.00×10^{-2}	2.47×10^{-2}	1.36×10^{-2}
0.0603-0.0494	1.64×10^{-3}	5.27×10^{-4}	2.09×10^{-4}	6.67×10^{-4}	8.86×10^{-4}	6.16×10^{-4}	6.72×10^{-3}	4.32×10^{-3}	6.55×10^{-4}

a. Averaged over the first 200 cm along the edge of the cylinder.

TABLE IV

Spatial Dependence of the Photon Dose Rates and Photon Leakage Fluxes for Selected Residual Nuclides Produced by 200-GeV Protons in an Iron Cylinder of 30.48-cm Radius Surrounded by 10.16 cm of Lead

Distance Along Cylinder (cm)	Photon Dose Rate[a] [(rem/h)/(incident 200-GeV proton/sec)]											
	^{204m}Pb	^{203}Pb	^{202m}Pb	^{201}Pb	^{200}Pb	^{199}Pb[b]	^{199m}Pb	^{198}Pb	^{202}Tl[b]	^{200}Tl[b]	^{199}Tl[b]	^{198}Tl[b]	^{198m}Tl
0- 25	5.37×10^{-12}	1.43×10^{-13}	2.49×10^{-12}	1.16×10^{-12}	1.94×10^{-14}	7.50×10^{-13}	1.61×10^{-14}	1.23×10^{-13}	1.15×10^{-13}	3.43×10^{-13}	1.19×10^{-14}	3.58×10^{-13}	5.09×10^{-14}
25- 50	1.37×10^{-11}	5.41×10^{-13}	6.97×10^{-12}	3.35×10^{-12}	8.46×10^{-14}	2.16×10^{-12}	5.62×10^{-14}	3.57×10^{-13}	3.98×10^{-13}	9.63×10^{-13}	4.57×10^{-14}	1.02×10^{-12}	1.68×10^{-13}
50- 75	1.73×10^{-11}	6.32×10^{-13}	8.32×10^{-12}	4.18×10^{-12}	1.05×10^{-13}	2.52×10^{-12}	7.61×10^{-14}	4.50×10^{-13}	4.30×10^{-13}	1.27×10^{-12}	4.92×10^{-14}	1.22×10^{-12}	1.97×10^{-13}
75-100	1.40×10^{-11}	6.19×10^{-13}	6.89×10^{-12}	4.58×10^{-12}	8.79×10^{-14}	2.10×10^{-12}	5.34×10^{-14}	3.62×10^{-13}	3.34×10^{-13}	1.02×10^{-12}	4.04×10^{-14}	9.91×10^{-13}	1.65×10^{-13}
100-125	1.17×10^{-11}	4.46×10^{-13}	5.44×10^{-12}	2.67×10^{-12}	5.68×10^{-14}	1.72×10^{-12}	4.76×10^{-14}	3.02×10^{-13}	2.94×10^{-13}	8.96×10^{-13}	3.33×10^{-14}	8.41×10^{-13}	1.22×10^{-13}
125-150	7.20×10^{-12}	2.93×10^{-13}	3.91×10^{-12}	1.90×10^{-12}	6.64×10^{-14}	1.12×10^{-12}	3.43×10^{-14}	1.82×10^{-13}	1.98×10^{-13}	6.30×10^{-13}	2.53×10^{-14}	5.11×10^{-13}	8.45×10^{-14}
150-175	4.52×10^{-12}	1.61×10^{-13}	2.24×10^{-12}	9.78×10^{-13}	2.06×10^{-14}	6.31×10^{-13}	1.53×10^{-14}	9.72×10^{-14}	1.21×10^{-13}	3.23×10^{-13}	1.09×10^{-14}	3.48×10^{-13}	4.90×10^{-14}
175-200	1.78×10^{-12}	4.04×10^{-14}	8.50×10^{-13}	4.20×10^{-13}	1.05×10^{-14}	2.21×10^{-13}	6.19×10^{-15}	3.26×10^{-14}	3.86×10^{-14}	1.41×10^{-13}	4.39×10^{-15}	1.37×10^{-13}	1.87×10^{-14}
Average	9.45×10^{-12}	3.60×10^{-13}	4.64×10^{-12}	2.41×10^{-12}	5.64×10^{-14}	1.40×10^{-12}	3.82×10^{-14}	2.38×10^{-13}	2.41×10^{-13}	6.98×10^{-13}	2.76×10^{-14}	6.78×10^{-13}	1.07×10^{-13}
Albedo	1.31×10^{-12}	3.51×10^{-14}	7.51×10^{-13}	2.92×10^{-13}	6.70×10^{-15}	1.71×10^{-13}	3.67×10^{-15}	2.88×10^{-14}	3.33×10^{-14}	1.10×10^{-13}	2.47×10^{-15}	7.36×10^{-14}	1.86×10^{-14}

Distance Along Cylinder (cm)	Photon Leakage Flux[a] [(photons/sec·cm^2)/(incident 200-GeV proton/sec)]											
	^{204m}Pb	^{203}Pb	^{202m}Pb	^{201}Pb	^{200}Pb	^{199}Pb[b]	^{199m}Pb	^{198}Pb	^{202}Tl[b]	^{200}Tl[b]	^{199}Tl[b]	^{198}Tl[b]	^{198m}Tl
0- 25	3.27×10^{-6}	1.94×10^{-7}	1.62×10^{-6}	7.96×10^{-7}	2.27×10^{-8}	3.84×10^{-7}	1.65×10^{-8}	1.04×10^{-7}	1.08×10^{-7}	1.94×10^{-7}	1.22×10^{-8}	1.66×10^{-7}	4.21×10^{-8}
25- 50	8.36×10^{-6}	7.26×10^{-7}	4.64×10^{-6}	2.33×10^{-6}	9.78×10^{-8}	1.14×10^{-6}	5.73×10^{-8}	3.32×10^{-7}	3.67×10^{-7}	5.58×10^{-7}	4.58×10^{-8}	4.67×10^{-7}	1.40×10^{-7}
50- 75	1.05×10^{-5}	8.41×10^{-7}	5.54×10^{-6}	2.91×10^{-6}	1.34×10^{-7}	1.34×10^{-6}	7.77×10^{-8}	4.30×10^{-7}	3.97×10^{-7}	7.14×10^{-7}	5.17×10^{-8}	5.79×10^{-7}	1.64×10^{-7}
75-100	8.58×10^{-6}	8.19×10^{-7}	4.57×10^{-6}	2.84×10^{-6}	1.09×10^{-7}	1.12×10^{-6}	5.46×10^{-8}	3.44×10^{-7}	3.08×10^{-7}	5.75×10^{-7}	4.40×10^{-8}	4.65×10^{-7}	1.40×10^{-7}
100-125	7.24×10^{-6}	6.00×10^{-7}	3.54×10^{-6}	1.82×10^{-6}	7.94×10^{-8}	9.16×10^{-7}	4.82×10^{-8}	2.74×10^{-7}	2.72×10^{-7}	5.00×10^{-7}	3.51×10^{-8}	3.87×10^{-7}	1.03×10^{-7}
125-150	4.54×10^{-6}	3.84×10^{-7}	2.60×10^{-6}	1.27×10^{-6}	7.62×10^{-8}	5.88×10^{-7}	3.47×10^{-8}	1.63×10^{-7}	1.83×10^{-7}	3.51×10^{-7}	2.74×10^{-8}	2.43×10^{-7}	7.14×10^{-8}
150-175	2.70×10^{-6}	2.21×10^{-7}	1.46×10^{-6}	6.74×10^{-7}	2.81×10^{-8}	3.39×10^{-7}	1.55×10^{-8}	8.58×10^{-8}	1.10×10^{-7}	1.80×10^{-7}	1.15×10^{-8}	1.62×10^{-7}	4.16×10^{-8}
175-200	1.06×10^{-6}	5.12×10^{-8}	5.54×10^{-7}	2.83×10^{-7}	9.79×10^{-9}	1.18×10^{-7}	6.29×10^{-9}	2.98×10^{-8}	3.62×10^{-8}	7.65×10^{-8}	4.49×10^{-9}	6.56×10^{-8}	1.51×10^{-8}
Average	5.78×10^{-6}	4.75×10^{-7}	3.07×10^{-6}	1.62×10^{-6}	6.96×10^{-8}	7.43×10^{-7}	3.89×10^{-8}	2.20×10^{-7}	2.23×10^{-7}	3.94×10^{-7}	2.90×10^{-8}	3.17×10^{-7}	8.97×10^{-8}
Albedo	8.15×10^{-7}	4.84×10^{-8}	5.08×10^{-7}	2.21×10^{-7}	8.82×10^{-9}	9.88×10^{-8}	3.79×10^{-9}	2.82×10^{-8}	3.16×10^{-8}	6.13×10^{-8}	2.70×10^{-9}	3.68×10^{-8}	1.74×10^{-8}
K	-	-	-	-	-	1.00	-	-	3.49	0.202	0.384	2.17, 0.200	-

a. Time of irradiation = infinite;
Time after shutdown = 0 (see footnote on page 18).

b. Does not include contribution from decaying nuclides; i.e., for example, $^{199m}Pb \rightarrow {}^{199}Pb$.

TABLE V

Energy Dependence of the Averaged Normalized Photon Leakage Fluxes Per Unit Energy for Selected Residual Nuclides Produced by 200-GeV Protons in an Iron Cylinder of 30.48-cm Radius Surrounded by 10.16 cm of Lead

Energy Interval (MeV)	Normalized Photon Leakage Flux Per Unit Energy[a] (MeV^{-1})												
	^{204m}Pb	^{203}Pb	^{202m}Pb	^{201}Pb	^{200}Pb	^{199}Pb	^{199m}Pb	^{198}Pb	^{202}Tl	^{200}Tl	^{199}Tl	^{198}Tl	^{198m}Tl
2.68 -2.20												7.50×10^{-2}	
2.20 -1.80						6.36×10^{-2}				3.25×10^{-2}		3.69×10^{-1}	
1.80 -1.47				4.44×10^{-2}		4.58×10^{-1}				1.53×10^{-1}		3.79×10^{-1}	
1.47 -1.21				3.51×10^{-1}		4.82×10^{-1}				5.26×10^{-1}		6.35×10^{-1}	
1.21 -0.988				4.14×10^{-1}		9.17×10^{-1}				1.18×10^{0}		5.99×10^{-1}	7.22×10^{-2}
0.988-0.809	3.81×10^{0}		2.13×10^{0}	1.21×10^{0}		4.69×10^{-1}		9.11×10^{-1}		6.82×10^{-1}		2.81×10^{-1}	1.35×10^{-2}
0.809-0.663	5.12×10^{-1}	1.91×10^{-1}	1.29×10^{0}	8.78×10^{-1}		8.98×10^{-1}		3.51×10^{-1}		4.05×10^{-1}		5.58×10^{-1}	8.93×10^{-2}
0.663-0.543	4.48×10^{-1}	7.87×10^{-2}	1.28×10^{0}	5.53×10^{-1}	4.44×10^{-1}	2.89×10^{-1}		9.68×10^{-1}		8.42×10^{-1}		4.84×10^{-1}	4.37×10^{0}
0.543-0.445	3.71×10^{-1}	2.46×10^{-2}	6.90×10^{-1}	2.51×10^{-1}	3.30×10^{0}	4.22×10^{-1}		3.23×10^{-1}	8.64×10^{0}	3.22×10^{-1}	6.44×10^{0}	3.80×10^{-1}	9.63×10^{-1}
0.445-0.364	1.27×10^{0}	1.06×10^{0}	2.09×10^{0}	3.43×10^{-1}	3.74×10^{-1}	1.85×10^{0}	1.13×10^{0}	3.90×10^{0}	9.72×10^{-1}	2.30×10^{0}	7.32×10^{-1}	1.74×10^{0}	2.52×10^{0}
0.364-0.298	5.38×10^{-1}	1.05×10^{-1}	3.22×10^{-1}	4.74×10^{0}	7.70×10^{-1}	6.54×10^{-1}	7.65×10^{-1}	4.00×10^{-1}	6.19×10^{-1}	3.18×10^{-1}	3.57×10^{-1}	2.25×10^{-1}	3.80×10^{-1}
0.298-0.244	1.60×10^{-1}	1.54×10^{1}	2.07×10^{-1}	2.85×10^{-1}	4.84×10^{0}	1.79×10^{-1}	4.26×10^{-1}	4.67×10^{0}	3.34×10^{-1}	2.02×10^{-1}	2.57×10^{0}	1.28×10^{-1}	1.89×10^{0}
0.244-0.200	9.46×10^{-2}	4.95×10^{-1}	1.41×10^{-1}	1.54×10^{-1}	1.78×10^{0}	6.43×10^{-2}	2.03×10^{-1}	3.00×10^{-1}	1.84×10^{-1}	1.09×10^{-1}	2.45×10^{0}	6.70×10^{-2}	3.45×10^{-1}
0.200-0.164	3.19×10^{-2}	3.04×10^{-1}	4.85×10^{-2}	7.54×10^{-2}	9.55×10^{-2}	2.94×10^{-2}	1.24×10^{-1}	8.46×10^{-1}	1.44×10^{-1}	7.04×10^{-2}	3.27×10^{-1}	2.74×10^{-2}	9.75×10^{-2}
0.164-0.134	3.87×10^{-3}	1.25×10^{-1}	8.27×10^{-3}	3.73×10^{-2}	6.54×10^{0}	6.51×10^{-3}	1.95×10^{-2}	4.64×10^{-2}	8.18×10^{-3}	8.96×10^{-3}	8.48×10^{-1}	8.37×10^{-3}	4.59×10^{-2}
0.134-0.110	1.73×10^{-3}	2.33×10^{-2}	1.25×10^{-3}	1.77×10^{-3}	9.95×10^{-2}	1.16×10^{-3}	2.16×10^{-3}	2.53×10^{-2}	1.15×10^{-3}	4.10×10^{-3}	1.99×10^{-2}	9.56×10^{-4}	3.83×10^{-3}
0.110-0.090	1.53×10^{-4}	8.88×10^{-4}	3.86×10^{-4}	2.42×10^{-4}	3.26×10^{-2}	1.09×10^{-4}	1.02×10^{-4}	1.43×10^{-3}	8.17×10^{-4}	9.74×10^{-5}	1.42×10^{-3}	3.35×10^{-4}	3.00×10^{-4}

a. Averaged over the first 200 cm along the edge of the cylinder.

TABLE VI

Average Photon Dose Rates and Photon Leakage Fluxes for Selected Residual Nuclides Produced by 200-GeV Protons in an Iron Cylinder of 30.48-cm Radius Surrounded by 5.08 cm of Lead

Element	Average Dose Rate[a] [(rem/h)/(incident 200-GeV proton/sec)]	Average Photon Leakage Flux[a] [(photons/sec•cm^2)/(incident 200-GeV proton/sec)]	K
^{56}Mn	1.64×10^{-12}	6.79×10^{-7}	
^{54}Mn	1.71×10^{-13}	1.14×10^{-7}	
^{52}Mn	5.03×10^{-13}	2.65×10^{-7}	
^{52m}Mn	4.05×10^{-13}	1.92×10^{-7}	
^{51}Mn	1.04×10^{-16}	9.91×10^{-11}	
^{49}Cr	4.84×10^{-17}	4.11×10^{-11}	
^{48}V	2.26×10^{-13}	1.11×10^{-7}	
^{44}Sc	1.60×10^{-14}	9.49×10^{-9}	
^{204m}Pb	1.48×10^{-11}	8.99×10^{-6}	
^{203}Pb	5.34×10^{-13}	7.19×10^{-7}	
^{202m}Pb	6.25×10^{-12}	4.09×10^{-6}	
^{201}Pb	3.06×10^{-12}	2.08×10^{-6}	
^{200}Pb	7.59×10^{-14}	9.44×10^{-8}	
^{199}Pb[b]	2.35×10^{-12}	1.26×10^{-6}	1.00
^{199m}Pb	6.45×10^{-14}	6.56×10^{-8}	
^{198}Pb	4.65×10^{-13}	4.23×10^{-7}	
^{202}Tℓ[b]	5.13×10^{-13}	4.72×10^{-7}	3.49
^{200}Tℓ[b]	1.07×10^{-12}	6.06×10^{-7}	0.202
^{199}Tℓ[b]	3.15×10^{-14}	3.29×10^{-8}	0.384
^{198}Tℓ[b]	1.34×10^{-12}	6.24×10^{-7}	2.17, 0.200
^{198m}Tℓ	2.20×10^{-13}	1.82×10^{-7}	

a. Time of irradiation = infinite;
Time after shutdown = 0 (see footnote on page 18).

b. Does not include contribution from decaying nuclides; i.e., for example, ^{199m}Pb → ^{199}Pb.

TABLE VII

Spatial Dependence of the Photon Dose Rates and Photon Leakage Fluxes for Selected Residual Nuclides Produced by 200-GeV Protons in an Iron Cylinder of 10.16-cm Radius

Distance Along Cylinder (cm)	Photon Dose Rate[a] [(rem/h)/(incident 200-GeV proton/sec)]							
	^{56}Mn	^{54}Mn	^{52}Mn	^{52m}Mn	^{51}Mn	^{49}Cr	^{48}V	^{44}Sc
0- 25	1.10×10^{-9}	8.96×10^{-10}	6.78×10^{-10}	4.63×10^{-10}	5.66×10^{-11}	2.41×10^{-11}	4.38×10^{-10}	7.81×10^{-12}
25- 50	2.35×10^{-9}	2.08×10^{-9}	1.73×10^{-9}	1.21×10^{-9}	1.39×10^{-10}	5.33×10^{-11}	1.27×10^{-9}	2.15×10^{-11}
50- 75	2.40×10^{-9}	2.14×10^{-9}	1.90×10^{-9}	1.33×10^{-9}	1.84×10^{-10}	7.16×10^{-11}	1.47×10^{-9}	2.66×10^{-11}
75-100	1.63×10^{-9}	1.56×10^{-9}	1.31×10^{-9}	9.44×10^{-10}	1.32×10^{-10}	5.03×10^{-11}	1.03×10^{-9}	1.81×10^{-11}
100-125	8.95×10^{-10}	9.15×10^{-10}	7.92×10^{-10}	5.58×10^{-10}	8.08×10^{-11}	3.28×10^{-11}	6.93×10^{-10}	1.23×10^{-11}
125-150	5.61×10^{-10}	5.79×10^{-10}	5.27×10^{-10}	3.48×10^{-10}	5.25×10^{-11}	1.85×10^{-11}	4.92×10^{-10}	8.43×10^{-12}
150-175	2.74×10^{-10}	3.00×10^{-10}	2.92×10^{-10}	1.81×10^{-10}	2.66×10^{-11}	1.23×10^{-11}	1.89×10^{-10}	3.50×10^{-12}
175-200	1.23×10^{-10}	1.08×10^{-10}	1.00×10^{-10}	7.55×10^{-11}	7.11×10^{-12}	2.56×10^{-12}	7.08×10^{-11}	1.26×10^{-12}
Average	1.17×10^{-9}	1.07×10^{-9}	9.16×10^{-10}	6.38×10^{-10}	8.50×10^{-11}	3.32×10^{-11}	7.05×10^{-10}	1.25×10^{-11}
Albedo	7.99×10^{-10}	8.38×10^{-10}	6.58×10^{-10}	3.98×10^{-10}	6.76×10^{-11}	2.91×10^{-11}	7.15×10^{-10}	1.31×10^{-11}
Distance Along Cylinder (cm)	Photon Leakage Flux[a] [(photons/sec•cm^2)/(incident 200-GeV proton/sec)]							
	^{56}Mn	^{54}Mn	^{52}Mn	^{52m}Mn	^{51}Mn	^{49}Cr	^{48}V	^{44}Sc
0- 25	6.85×10^{-4}	7.39×10^{-4}	5.04×10^{-4}	3.68×10^{-4}	6.49×10^{-5}	2.86×10^{-5}	3.38×10^{-4}	6.15×10^{-6}
25- 50	1.47×10^{-3}	1.69×10^{-3}	1.27×10^{-3}	9.36×10^{-4}	1.63×10^{-4}	6.13×10^{-5}	9.68×10^{-4}	1.52×10^{-5}
50- 75	1.48×10^{-3}	1.73×10^{-3}	1.34×10^{-3}	9.95×10^{-4}	2.04×10^{-4}	8.05×10^{-5}	1.08×10^{-3}	1.92×10^{-5}
75-100	9.87×10^{-4}	1.27×10^{-3}	9.35×10^{-4}	7.31×10^{-4}	1.45×10^{-4}	5.46×10^{-5}	7.59×10^{-4}	1.23×10^{-5}
100-125	5.57×10^{-4}	7.25×10^{-4}	5.61×10^{-4}	4.21×10^{-4}	8.99×10^{-5}	3.66×10^{-5}	4.99×10^{-4}	8.69×10^{-6}
125-150	3.51×10^{-4}	4.55×10^{-4}	3.76×10^{-4}	2.73×10^{-4}	5.90×10^{-5}	2.16×10^{-5}	3.51×10^{-4}	6.13×10^{-6}
150-175	1.67×10^{-4}	2.38×10^{-4}	2.04×10^{-4}	1.36×10^{-4}	3.00×10^{-5}	1.21×10^{-5}	1.37×10^{-4}	2.54×10^{-6}
175-200	7.74×10^{-5}	8.78×10^{-5}	7.08×10^{-5}	5.66×10^{-5}	8.11×10^{-6}	2.81×10^{-6}	5.19×10^{-5}	8.24×10^{-7}
Average	7.24×10^{-4}	8.69×10^{-4}	6.58×10^{-4}	4.90×10^{-4}	9.56×10^{-5}	3.73×10^{-5}	5.23×10^{-4}	8.88×10^{-6}
Albedo	5.77×10^{-4}	6.52×10^{-4}	4.72×10^{-4}	3.06×10^{-4}	7.91×10^{-5}	3.37×10^{-5}	5.24×10^{-4}	7.58×10^{-6}

a. Time of irradiation = infinite;
Time after shutdown = 0 (see footnote on page 18).

TABLE VIII

Spatial Dependence of the Photon Dose Rates and Photon Leakage Fluxes for Selected Residual Nuclides Produced by 200-GeV Protons in an Iron Cylinder of 20.32-cm Radius

Distance Along Cylinder (cm)	Photon Dose Rate[a] [(rem/h)/(incident 200-GeV proton/sec)]							
	^{56}Mn	^{54}Mn	^{52}Mn	^{52m}Mn	^{51}Mn	^{49}Cr	^{48}V	^{44}Sc
0- 25	1.91×10^{-10}	1.49×10^{-10}	9.44×10^{-11}	6.05×10^{-11}	9.22×10^{-12}	3.21×10^{-12}	4.41×10^{-11}	2.93×10^{-12}
25- 50	4.11×10^{-10}	3.73×10^{-10}	2.54×10^{-10}	1.83×10^{-10}	2.01×10^{-11}	7.82×10^{-12}	1.12×10^{-10}	7.18×10^{-12}
50- 75	5.36×10^{-10}	4.91×10^{-10}	3.35×10^{-10}	2.43×10^{-10}	3.01×10^{-11}	1.22×10^{-11}	1.87×10^{-10}	1.16×10^{-11}
75-100	4.26×10^{-10}	3.69×10^{-10}	2.83×10^{-10}	2.07×10^{-10}	2.85×10^{-11}	1.09×10^{-11}	1.64×10^{-10}	1.04×10^{-11}
100-125	2.53×10^{-10}	2.47×10^{-10}	1.87×10^{-10}	1.30×10^{-10}	1.87×10^{-11}	6.51×10^{-12}	1.08×10^{-10}	6.63×10^{-12}
125-150	1.45×10^{-10}	1.70×10^{-10}	9.35×10^{-11}	6.18×10^{-11}	8.39×10^{-12}	3.31×10^{-12}	4.79×10^{-11}	3.32×10^{-12}
150-175	9.85×10^{-11}	8.52×10^{-11}	5.87×10^{-11}	4.71×10^{-11}	6.63×10^{-12}	2.31×10^{-12}	3.92×10^{-11}	2.48×10^{-12}
175-200	4.22×10^{-11}	4.97×10^{-11}	4.67×10^{-11}	2.29×10^{-11}	3.72×10^{-12}	1.41×10^{-12}	2.40×10^{-11}	1.21×10^{-12}
Average	2.63×10^{-10}	2.42×10^{-10}	1.69×10^{-10}	1.20×10^{-10}	1.57×10^{-11}	5.95×10^{-12}	9.08×10^{-11}	5.72×10^{-12}
Albedo	3.31×10^{-10}	2.73×10^{-10}	2.43×10^{-10}	1.37×10^{-10}	2.58×10^{-11}	1.01×10^{-11}	2.20×10^{-10}	1.47×10^{-11}

Distance Along Cylinder (cm)	Photon Leakage Flux[a] [(photons/sec·cm^2)/(incident 200-GeV proton/sec)]							
	^{56}Mn	^{54}Mn	^{52}Mn	^{52m}Mn	^{51}Mn	^{49}Cr	^{48}V	^{44}Sc
0- 25	1.17×10^{-4}	1.21×10^{-4}	6.79×10^{-5}	4.53×10^{-5}	9.76×10^{-6}	3.45×10^{-6}	3.28×10^{-5}	2.23×10^{-6}
25- 50	2.54×10^{-4}	3.01×10^{-4}	1.82×10^{-4}	1.41×10^{-4}	2.28×10^{-5}	8.95×10^{-6}	8.61×10^{-5}	5.41×10^{-6}
50- 75	3.24×10^{-4}	3.88×10^{-4}	2.38×10^{-4}	1.80×10^{-4}	3.28×10^{-5}	1.25×10^{-5}	1.34×10^{-4}	8.62×10^{-6}
75-100	2.61×10^{-4}	2.94×10^{-4}	2.05×10^{-4}	1.57×10^{-4}	3.14×10^{-5}	1.21×10^{-5}	1.16×10^{-4}	7.13×10^{-6}
100-125	1.57×10^{-4}	1.95×10^{-4}	1.29×10^{-4}	1.03×10^{-4}	2.08×10^{-5}	7.11×10^{-6}	8.01×10^{-5}	4.62×10^{-6}
125-150	8.91×10^{-5}	1.38×10^{-4}	7.28×10^{-5}	4.89×10^{-5}	9.32×10^{-6}	3.72×10^{-6}	3.49×10^{-5}	2.42×10^{-6}
150-175	6.05×10^{-5}	6.83×10^{-5}	4.16×10^{-5}	3.29×10^{-5}	7.35×10^{-6}	2.49×10^{-6}	2.83×10^{-5}	1.85×10^{-6}
175-200	2.47×10^{-5}	3.83×10^{-5}	2.94×10^{-5}	1.83×10^{-5}	3.85×10^{-6}	1.46×10^{-6}	1.60×10^{-5}	8.51×10^{-7}
Average	1.61×10^{-4}	1.93×10^{-4}	1.21×10^{-4}	9.08×10^{-5}	1.73×10^{-5}	6.47×10^{-6}	6.73×10^{-5}	4.14×10^{-6}
Albedo	2.01×10^{-4}	2.19×10^{-4}	1.69×10^{-4}	1.04×10^{-4}	2.77×10^{-5}	1.09×10^{-5}	1.59×10^{-4}	9.92×10^{-6}

a. Time of irradiation = infinite;
Time after shutdown = 0 (see footnote on page 18).

TABLE IX

Spatial Dependence of the Photon Dose Rates and Photon Leakage Fluxes for Selected Residual Nuclides Produced by 200-GeV Protons in an Iron Cylinder of 30.48-cm Radius

Distance Along Cylinder (cm)	Photon Dose Rate[a] [(rem/h)/(incident 200-GeV proton/sec)]							
	^{56}Mn	^{54}Mn	^{52}Mn	^{52m}Mn	^{51}Mn	^{49}Cr	^{48}V	^{44}Sc
0- 25	8.18×10^{-11}	5.91×10^{-11}	4.46×10^{-11}	2.42×10^{-11}	3.21×10^{-12}	1.15×10^{-12}	1.64×10^{-11}	1.11×10^{-12}
25- 50	1.26×10^{-10}	1.08×10^{-10}	7.68×10^{-11}	5.02×10^{-11}	7.26×10^{-12}	2.72×10^{-12}	3.56×10^{-11}	2.38×10^{-12}
50- 75	1.52×10^{-10}	1.55×10^{-10}	1.36×10^{-10}	9.08×10^{-11}	9.37×10^{-12}	3.25×10^{-12}	5.39×10^{-11}	3.24×10^{-12}
75-100	1.51×10^{-10}	1.28×10^{-10}	9.12×10^{-11}	6.87×10^{-11}	7.69×10^{-12}	2.61×10^{-12}	3.70×10^{-11}	2.51×10^{-12}
100-125	1.21×10^{-10}	1.01×10^{-10}	8.08×10^{-11}	6.16×10^{-11}	6.65×10^{-12}	2.52×10^{-12}	3.69×10^{-11}	2.33×10^{-12}
125-150	6.41×10^{-11}	6.82×10^{-11}	5.55×10^{-11}	3.63×10^{-11}	4.37×10^{-12}	1.58×10^{-12}	1.38×10^{-11}	9.65×10^{-13}
150-175	3.56×10^{-11}	3.56×10^{-11}	2.60×10^{-11}	2.00×10^{-11}	2.50×10^{-12}	8.84×10^{-13}	1.54×10^{-11}	7.41×10^{-13}
175-200	1.68×10^{-11}	2.23×10^{-11}	1.50×10^{-11}	8.81×10^{-12}	1.41×10^{-12}	5.21×10^{-13}	1.06×10^{-11}	6.61×10^{-13}
Average	9.36×10^{-11}	8.46×10^{-11}	6.59×10^{-11}	4.51×10^{-11}	5.31×10^{-12}	1.91×10^{-12}	2.74×10^{-11}	1.75×10^{-12}
Albedo	1.79×10^{-10}	1.48×10^{-10}	9.36×10^{-11}	6.62×10^{-11}	1.27×10^{-11}	4.62×10^{-12}	1.38×10^{-10}	8.91×10^{-12}

Distance Along Cylinder (cm)	Photon Leakage Flux[a] [(photons/sec•cm^2)/(incident 200-GeV proton/sec)]							
	^{56}Mn	^{54}Mn	^{52}Mn	^{52m}Mn	^{51}Mn	^{49}Cr	^{48}V	^{44}Sc
0- 25	4.74×10^{-5}	4.67×10^{-5}	2.92×10^{-5}	2.03×10^{-5}	3.41×10^{-6}	1.25×10^{-6}	1.14×10^{-5}	7.69×10^{-7}
25- 50	7.90×10^{-5}	8.57×10^{-5}	5.69×10^{-5}	3.85×10^{-5}	7.77×10^{-6}	2.95×10^{-6}	2.49×10^{-5}	1.75×10^{-6}
50- 75	9.12×10^{-5}	1.22×10^{-4}	9.24×10^{-5}	6.83×10^{-5}	1.01×10^{-5}	3.41×10^{-6}	4.09×10^{-5}	2.51×10^{-6}
75-100	9.71×10^{-5}	1.01×10^{-4}	6.45×10^{-5}	5.13×10^{-5}	8.18×10^{-6}	2.75×10^{-6}	2.67×10^{-5}	1.71×10^{-6}
100-125	6.85×10^{-5}	8.05×10^{-5}	5.57×10^{-5}	4.59×10^{-5}	7.73×10^{-6}	2.81×10^{-6}	2.67×10^{-5}	1.62×10^{-6}
125-150	4.02×10^{-5}	5.40×10^{-5}	4.14×10^{-5}	2.60×10^{-5}	4.86×10^{-6}	1.61×10^{-6}	9.93×10^{-6}	7.12×10^{-7}
150-175	2.19×10^{-5}	3.03×10^{-5}	1.88×10^{-5}	1.48×10^{-5}	2.79×10^{-6}	9.77×10^{-7}	1.10×10^{-5}	5.32×10^{-7}
175-200	1.04×10^{-5}	1.65×10^{-5}	1.10×10^{-5}	7.37×10^{-5}	1.57×10^{-6}	5.81×10^{-7}	8.21×10^{-6}	5.01×10^{-7}
Average	5.70×10^{-5}	6.71×10^{-5}	4.62×10^{-5}	3.41×10^{-5}	5.80×10^{-6}	2.04×10^{-6}	2.00×10^{-5}	1.26×10^{-6}
Albedo	1.08×10^{-4}	1.15×10^{-4}	6.87×10^{-5}	5.00×10^{-5}	1.40×10^{-5}	5.11×10^{-6}	1.08×10^{-4}	6.91×10^{-6}

a. Time of irradiation = infinite;
Time after shutdown = 0 (see footnote on page 18).

TABLE X

Energy Dependence of the Averaged Normalized Photon Leakage Flux Per Unit Energy for Selected Residual Nuclides Produced by 200-GeV Protons in an Iron Cylinder of 20.32-cm Radius

Energy Interval (MeV)	Normalized Photon Leakage Flux Per Unit Energy[a] (MeV^{-1})						
	^{56}Mn	^{54}Mn	^{52}Mn	^{52m}Mn	^{51}Mn	^{49}Cr	^{48}V
4.00 -3.28	8.30×10^{-4}						
3.28 -2.68	4.40×10^{-3}						
2.68 -2.20	2.45×10^{-2}						8.70×10^{-3}
2.20 -1.80	2.83×10^{-1}						6.45×10^{-3}
1.80 -1.47	1.87×10^{-1}			1.30×10^{-1}			3.28×10^{-3}
1.47 -1.21	9.72×10^{-2}		6.40×10^{-1}	6.14×10^{-1}			5.18×10^{-1}
1.21 -0.988	1.03×10^{-1}		1.41×10^{-1}	1.49×10^{-1}			4.05×10^{-1}
0.988 -0.809	1.37×10^{0}	1.72×10^{0}	7.80×10^{-1}	1.69×10^{-1}			7.54×10^{-1}
0.809 -0.663	5.94×10^{-1}	1.06×10^{0}	8.77×10^{-1}	1.86×10^{-1}			3.96×10^{-1}
0.663 -0.543	5.24×10^{-1}	6.98×10^{-1}	5.08×10^{-1}	2.39×10^{-1}			4.32×10^{-1}
0.543 -0.445	6.83×10^{-1}	8.81×10^{-1}	1.07×10^{0}	2.65×10^{0}	4.68×10^{0}	4.88×10^{0}	1.38×10^{0}
0.445 -0.364	7.25×10^{-1}	8.13×10^{-1}	8.58×10^{-1}	1.11×10^{0}	1.45×10^{0}	1.06×10^{0}	9.23×10^{-1}
0.364 -0.298	7.77×10^{-1}	1.09×10^{0}	9.67×10^{-1}	1.10×10^{0}	1.58×10^{0}	1.59×10^{0}	1.15×10^{0}
0.298 -0.244	1.02×10^{0}	1.29×10^{0}	1.31×10^{0}	1.52×10^{0}	1.59×10^{0}	1.67×10^{0}	1.21×10^{0}
0.244 -0.200	1.23×10^{0}	1.44×10^{0}	1.33×10^{0}	1.46×10^{0}	1.75×10^{0}	1.41×10^{0}	1.36×10^{0}
0.200 -0.164	8.65×10^{-1}	1.33×10^{0}	1.27×10^{0}	1.33×10^{0}	2.13×10^{0}	2.17×10^{0}	1.46×10^{0}
0.164 -0.134	9.75×10^{-1}	8.31×10^{-1}	1.08×10^{0}	1.13×10^{0}	1.44×10^{0}	1.39×10^{0}	9.91×10^{-1}
0.134 -0.110	5.91×10^{-1}	6.97×10^{-1}	7.45×10^{-1}	6.96×10^{-1}	1.01×10^{0}	1.25×10^{0}	7.16×10^{-1}
0.110 -0.0900	2.88×10^{-1}	3.26×10^{-1}	2.76×10^{-1}	3.34×10^{-1}	4.29×10^{-1}	8.60×10^{-1}	3.91×10^{-1}
0.0900-0.0737	8.25×10^{-2}	8.65×10^{-2}	9.98×10^{-2}	1.15×10^{-1}	1.39×10^{-1}	3.01×10^{-1}	1.08×10^{-1}
0.0737-0.0603	9.71×10^{-3}	1.96×10^{-2}	7.17×10^{-3}	1.84×10^{-2}	2.23×10^{-2}	3.50×10^{-2}	1.24×10^{-2}
0.0603-0.0494	7.58×10^{-4}	7.61×10^{-4}	6.89×10^{-4}	8.59×10^{-4}	2.66×10^{-3}	8.61×10^{-3}	5.44×10^{-4}

a. Averaged over the first 200 cm along the edge of the cylinder.

The beam stop for these data is composed entirely of iron. Data corresponding to the results presented in Table II are given in Tables VII–IX for radii of 10.16, 20.32, and 30.48 cm, respectively. The normalized photon leakage spectrum is given in Table X for only the 20.32-cm-radius case because of the similarity in these data and the data for the 10.16- and 30.48-cm cases. As with case 2, the same HETC transport results for the 40.64-cm beam stop were used for the beam stops of smaller radii by removing from consideration in the photon transport the appropriate amount of iron.

SUMMARY

These calculations indicate that the photon dose rate surrounding an iron beam stop can be substantially reduced by replacing the outer few inches of iron with lead. This reduction in dose rate results from several considerations. The half-lives of the radioactive nuclides produced in the lead are, for the most part, shorter than those produced in the iron. Therefore, since a majority of the photon dose comes from those nuclides produced near the edge, this difference in half-life results in a more rapid cooling time for the iron–lead shield. Also, the self-shielding characteristics of the lead, as compared to a similar amount of iron, allows for a far greater reduction in photon leakage and therefore a greater reduction in the photon dose rate.

ACKNOWLEDGEMENTS

The authors wish to thank Dr. M. Awschalom of the National Accelerator Laboratory for suggesting this study and Dr. R. G. Alsmiller, Jr. of the Oak Ridge National Laboratory for his helpful comments and encouragement throughout the work. We are also grateful to Dr. F. E. Bertrand and other members of the Nuclear Data Project of the Oak Ridge National Laboratory for their assistance in providing the most recent compilations of radioactive decay schemes used in the study.

REFERENCES

1. K. C. Chandler and T. W. Armstrong, 'Operating Instructions for the High-Energy Nucleon-Meson Transport Code HETC,' Oak Ridge National Laboratory Report ORNL-4744 (1972).
2. H. W. Bertini *et al.*, 'Instructions for the Operation of Codes Associated with MECC-3, a Preliminary Version of an Intranuclear-Cascade Calculation for Nuclear Reactions,' Oak Ridge National Laboratory Report ORNL-4564 (1971).
3. T. A. Gabriel, R. G. Alsmiller, Jr., and M. P. Guthrie, 'An Extrapolation Method for Predicting Nucleon and Pion Differential Production Cross Sections from High-Energy (> 3 GeV) Nucleon-Nucleus Collisions,' Oak Ridge National Laboratory Report ORNL-4542 (1970).
4. Hugo W. Bertini, Miriam P. Guthrie, and Arline H. Culkowski, 'Phenomenologically Determined Isobar Angular Distributions for Nucleon-Nucleon and Pion-Nucleon Reactions Below 3 GeV,' Oak Ridge National Laboratory Report ORNL-TM-3132 (1970).
5. T. A. Gabriel, R. T. Santoro, and J. Barish, 'A Calculational Method for Predicting Particle Spectra from High-Energy Nucleon and Pion Collisions ($\geqq$ 3 GeV) with Protons,' Oak Ridge National Laboratory Report ORNL-TM-3615 (1971).
6. E. A. Straker *et al.*, 'The MORSE Code—a Multigroup Neutron and Gamma-Ray Monte Carlo Transport Code,' Oak Ridge National Laboratory Report ORNL-4585 (1970).
7. L. R. Williams, Oak Ridge National Laboratory, private communication (1972).
8. R. Q. Wright *et al.*, 'Supertog: a Program to Generate Fine Group Constants and P_n Scattering Matrices from ENDF/B,' Oak Ridge National Laboratory Report ORNL-TM-2679 (1969).
9. J. R. Knight and F. R. Mynatt, 'MUG, a Program for Generating Multigroup Photon Cross Sections,' Computing Technology Center Report CTC-17, Union Carbide Corporation (1970).
10. S. K. Penny, D. K. Trubey, and M. B. Emmett, 'OGRE, a Monte Carlo System for Gamma-Ray Transport Studies, Including an Example (OGRE-P1) for Transmission Through Laminated Slabs,' Oak Ridge National Laboratory Report ORNL-3805 (1966).
11. M. D. Goldberg *et al.*, 'Neutron Cross Sections, Volume 11A, Z = 21 to 40,' Brookhaven National Laboratory Report BNL-325, Second Edition, Supplement 2 (1966).
12. Nuclear Data Sheets: **4**, Nos. 3–4, July 1970; **3**, Nos. 5, 6, April 1970; **3**, Nos. 3–4, January 1970; **6**, No. 4, October 1971; **5**, No. 6, June 1971; **7**, No. 4, April 1972; **5**, No. 5, May 1971. See also C. M. Lederer, J. M. Hollander, and I. Perlman, *Table of Isotopes*, sixth edition, John Wiley & Sons, Inc. (1967).
13. H. C. Claiborne and D. K. Trubey, 'Dose Rates in a Slab Phantom from Monoenergetic Gamma Rays,' Oak Ridge National Laboratory Report ORNL-TM-2574 (1969).
14. T. A. Gabriel and R. T. Santoro, 'Photon Dose Rates from the Interactions of 200-GeV Protons in Iron and Iron-Lead Beam Stops,' Oak Ridge National Laboratory Report ORNL-TM-3945 (1972).

Received 16 October 1972;
and in final form 11 December 1972